

## HETEROEPITAXIAL GROWTH OF $\text{LiTaO}_3$ THIN FILMS BY PYROSOL PROCESS

V. BORNAND<sup>a,\*</sup>, D. CHATEIGNER<sup>b</sup>, PH. PAPET<sup>a</sup>  
and E. PHILIPPOT<sup>a</sup>

<sup>a</sup> *Laboratoire de Physicochimie de la Matière Condensée  
UMR CNRS 5617, UM II Place Eugène Bataillon, CC003,  
F-34095 MONTPELLIER Cédex 5 France;*

<sup>b</sup> *Laboratoire de Physique de l'Etat Condensé, Université du Maine,  
Avenue Olivier Messiaen, F-72085 LE MANS Cédex 9 France*

(Received 5 November 1997)

Highly oriented  $\text{LiTaO}_3$  thin films were grown on (001) sapphire substrates by pyrosol process. X-ray diffraction analysis shows that the  $\text{LiTaO}_3$  crystallite *c*-axis is normal to the sapphire substrate. X-ray pole figures reveal that the films are also in-plane oriented, with two components of heteroepitaxy, the main one being stabilized with the  $\langle 110 \rangle$  axes of the layer parallel to the  $[110]$  direction of the substrate. Texture components are quantified.

*Keywords:*  $\text{LiTaO}_3$  thin films; chemical vapour deposition; deposition process; pyrolysis; X-ray diffraction

### INTRODUCTION

Because of their good piezoelectric and electrooptic properties,  $\text{LiTaO}_3$ -type ferroelectrics are technologically important for electrooptic, non-linear optical and surface acoustic waves devices. Thin films of  $\text{LiTaO}_3$  have been formed by many physical and chemical routes, such as rf-magnetron sputtering<sup>[1]</sup>, pulsed-laser deposition<sup>[2]</sup> and sol-gel methods.<sup>[3,4]</sup> Recently, we reported the successful growth of polycrystalline  $\text{LiTaO}_3$  layers on Si(111) substrates, and *c*-oriented  $\text{LiTaO}_3$  layers on  $\text{SiO}_2$ -coated Si(111) and  $\text{Al}_2\text{O}_3$  (006) substrates by

---

\* Corresponding author.

pyrosol process.<sup>[5]</sup> In this paper, we extend this work and provide additional insight into in-plane organization of the layers deposited on sapphire substrates.

## EXPERIMENTAL

The experimental setup of the pyrosol process deposition has been described earlier.<sup>[5]</sup> This system differs from conventional chemical vapour deposition system in its liquid delivery mechanism. An aerosol, generated by ultrasonic spraying of a precursor solution, is then conveyed by carrier gas near the surface of the heated substrates, giving rise to evaporation/pyrolysis process. A summary of the explored deposition conditions is presented in Table I. The crystallographic orientations of the films were determined by X-ray diffraction ( $\theta/2\theta$  spectra) and X-ray pole figure analyses. The used experimental set up, corrections for background, defocusing, absorption and volume variations were described earlier<sup>[6]</sup>, so was the quantifying methodology for integration and volumic proportion calculations.<sup>[7]</sup> The measurement of the full width at half-maximum (FWHM) of the rocking curves was also used as a measure of the crystalline quality of the films.

## RESULTS AND DISCUSSION

At first, we examined the experimental parameters to obtain crystallized and oriented films of  $\text{LiTaO}_3$  on (001) sapphire substrates.

TABLE I Deposition parameters

Solution	Precursors:	lithium acetylacetonate 99% (LANCASTER) tantalum ethoxide 99% (FLUKA)
	Solvent:	Methanol
	Concentration:	[Li] = 0.01 mol/l Li/Ta = 0.7
Spray parameters	Generator frequency:	800 kHz
	Generator power:	90 W
Carrier gas		dry air
	Rate:	170 l/h – 180 l/h
Substrates		sapphire $\text{Al}_2\text{O}_3(006)$
	Temperatures:	550°C to 660°C
	Growth rate:	10 – 12 nm/h

Because of their similar packing structure of atoms (Tab. II), highly oriented LiTaO<sub>3</sub> thin films can be expected to grow on Al<sub>2</sub>O<sub>3</sub> substrates. However, the substrate temperature during deposition represents one of the most important parameters affecting the film morphology (homogeneity and thickness) and crystallinity (single crystal or polycrystal). At substrate temperatures below 600°C, polycrystalline layers are obtained without any detectable parasitic phases by X-ray diffraction. However, they already present a strong orientation along the (001) direction as shown by the high values of the  $f(006)$  Lotgering factor<sup>[8]</sup> around 0.8. These  $f$  values, calculated from the maximum intensities of the XRD patterns for the (001) direction, can be considered as a measure of the degree of orientation along the normal to the substrate. A multiple-step deposition process, involving the successive deposition of LiTaO<sub>3</sub> layers (and different cycles in temperature) can improve this degree of orientation. For a substrate temperature of 590°C, it rises from 0.82 for a one-step deposition of 8 hours (Fig. 1a) to 0.86 for a two-steps deposition of 2×8 hours (Fig. 1b), showing that the quality of the film depends, to a large extent, on the physical properties of the underlying substrate.

X-ray diffraction patterns for films grown at substrate temperatures above 600°C show only peaks belonging to (001) LiTaO<sub>3</sub>, indicating that a strong preferential orientation with the {001} lithium tantalate planes parallel to the {001} sapphire ones (Fig. 2) is stabilized. A little substrate misorientation (during X-ray experiments) explains why we observe the X-ray peak of the substrate in the spectrum presented in Figure 2. Rocking curve analyses are consistent with improved crystallinity when the temperature is increased (Fig. 3). Furthermore, for a given temperature in the range 600°C–650°C, the use of a multiple-step deposition process allows a significant decrease of the FWHM around 0.3°, carrying out the proof of an improved quality of

TABLE II Structure and lattice parameters of LiTaO<sub>3</sub> and Al<sub>2</sub>O<sub>3</sub> (data from ASTM standards)

	Structure	Space group	Parameters
LiTaO <sub>3</sub>	Hexagonal (rhombohedral)	R3c	$a_H = 5.154 \text{ \AA}$ $c_H = 13.755 \text{ \AA}$ ( $a_R = 5.474 \text{ \AA}$ $\alpha_R = 56^\circ 10.5'$ )
Al <sub>2</sub> O <sub>3</sub>	Hexagonal (rhombohedral)	R $\bar{3}c$	$a_H = 4.758 \text{ \AA}$ $c_H = 12.991 \text{ \AA}$ ( $a_R = 5.12 \text{ \AA}$ $\alpha_R = 56^\circ 17'$ )

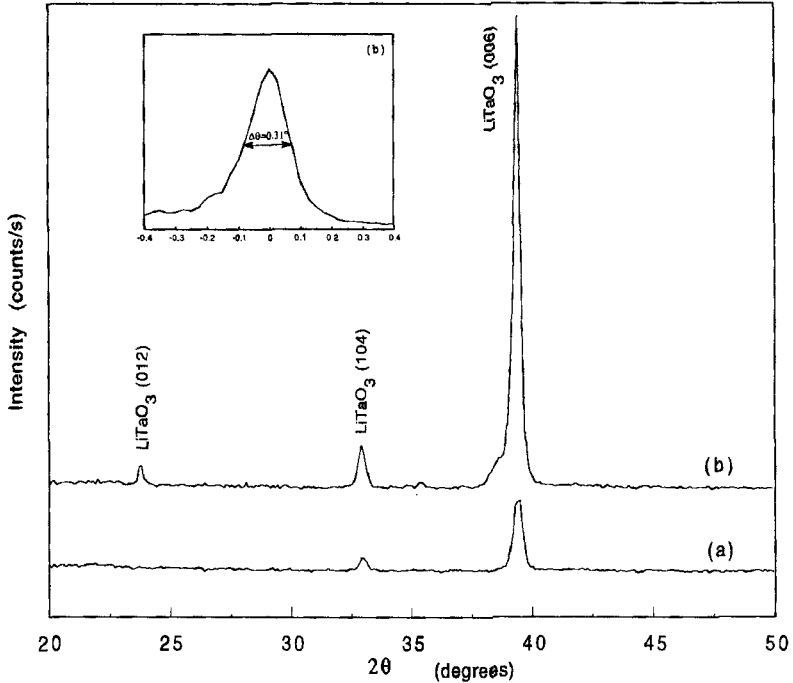


FIGURE 1 X-ray diffraction patterns and (006) rocking curve insert of  $\text{LiTaO}_3$  thin films deposited at  $580^\circ\text{C}$  on a  $c$ -oriented sapphire substrate, with initial liquid concentration of  $[\text{Li}] = 0.01 \text{ mol/l}$  and  $\text{Li/Ta} = 0.7$  (a) one-step deposition process (b) two-steps deposition process. Intensity scale is shifted for a better visualization of (a) and (b) spectra.

the as-grown films. The sapphire substrate, by itself, has a  $0.2^\circ$  FWHM for the same geometry. The larger the thickness of the layer is (*i.e.*, the less the substrate influences the layer), the better the crystalline quality and the homogeneity are. The systematic improvement of the crystalline quality of the films with their thickness implies that the surface of the latter becomes less defective, and hence a more effective template for epitaxy. This result is consistent with previously published results on  $\text{LiTaO}_3$  thin films grown on  $\text{Al}_2\text{O}_3$  substrates by pulsed laser deposition.<sup>[9]</sup> The lower quality of the near interface region is likely related to the misfit dislocations arising from a lattice mismatch of about 8%.

X-ray pole figures were measured by the reflection technique<sup>[10]</sup> and projected on the surface of a sample elaborated in optimized

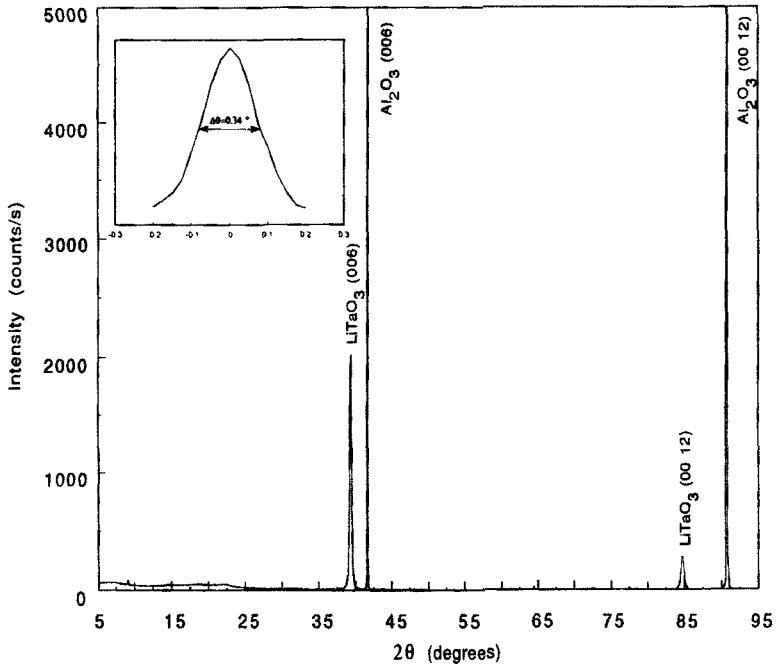


FIGURE 2 X-ray diffraction pattern and (006) rocking curve insert of a 150-nm thick  $\text{LiTaO}_3$  thin film synthesized by a one-step deposition process on a  $c$ -oriented sapphire substrate, at  $640^\circ\text{C}$ , with initial liquid concentration of  $[\text{Li}] = 0.01 \text{ mol/l}$  and  $\text{Li/Ta} = 0.7$ .

conditions. They confirm the strong preferred orientations of the crystallites and they reveal heteroepitaxial relationships (Fig. 4). We investigated a 150-nm thick  $\text{LiTaO}_3$  thin film grown on a  $c$ -oriented sapphire substrate. The position of the pole in the  $\{006\}$  pole figure, well centered, shows that all the crystallites have their  $c$ -axes perpendicular to the surface of the sample, thus parallel to the  $c$ -axis of the substrate ( $c_\perp$  orientation).  $\{012\}$  and  $\{104\}$  pole figures reveal strong in-plane orientation of the layer: most of the crystallites have their  $\langle 110 \rangle$  direction parallel to the  $[110]$  direction of the substrate, as shown by the high value of the pole density. For the  $\{012\}$  pole figure, we found  $D_{012}^{\text{max}}$  around 350 m.r.d. (multiple of a random distribution). However, we can identify two sets of poles,  $60^\circ$ -rotated one with respect to the other around their  $c$ -axes, evidencing two symmetrical in-plane orientations of the crystallites. In addition to the three poles of the dominant orientation that overlap with the substrate,

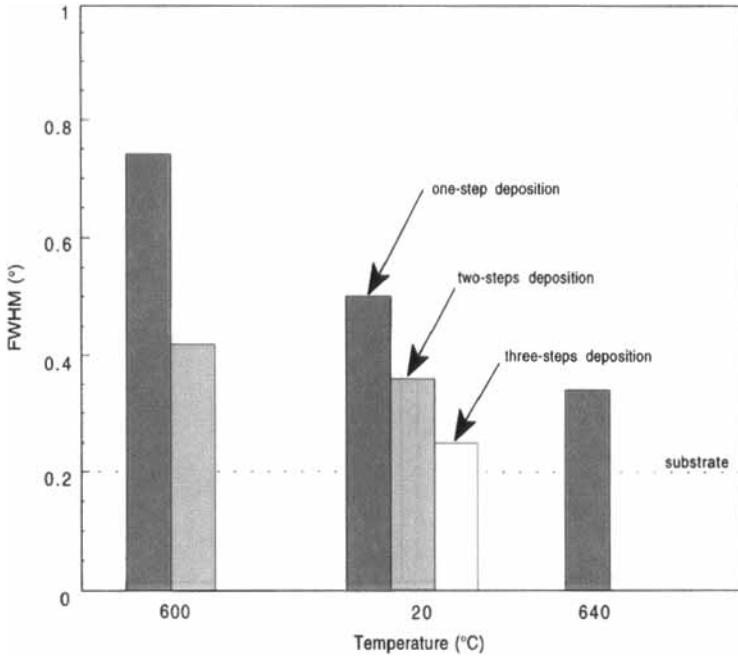


FIGURE 3 FWHM of the (006) rocking curve with respect to sapphire substrate temperature and deposition process.

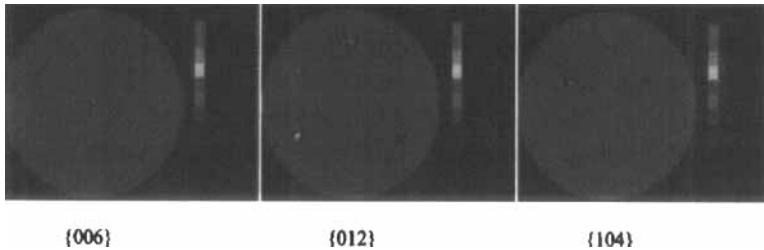


FIGURE 4 {006}, {012} and {104} pole figures of a 150-nm thick  $\text{LiTaO}_3$  thin film synthesized by a three-steps deposition process on a *c*-oriented sapphire substrate, at 610°C, with initial liquid concentration of  $[\text{Li}] = 0.01 \text{ mol/l}$  and  $\text{Li/Ta} = 0.7$ . Equal area projections, logarithmic intensity scale. (See Color Plate 1).

the sample shows three weaker poles (Fig. 5). The volumic ratio of crystallites of each orientation is not equal, the major orientation  $c_{\perp 0}$  being in exact alignment with the substrate. Figure 6 is a detailed view of the {012} pole figure of the same sample represented as a series of

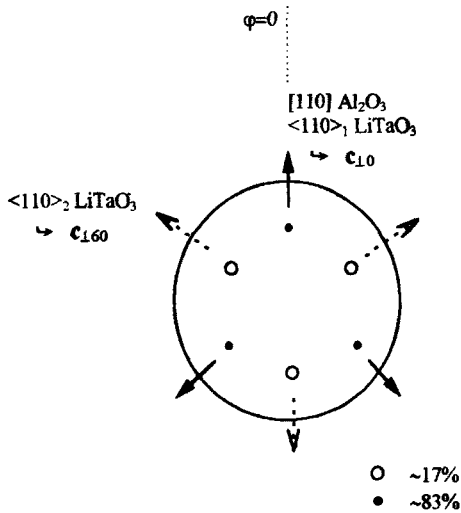


FIGURE 5 Detailed schema of the  $\{012\}$  pole figure of the Figure 4.

$\varphi$ -scans. The horizontal and depth axes are respectively the  $\varphi$  and  $\chi$  angles ( $0 \leq \varphi \leq 360^\circ$ ,  $44^\circ \leq \chi \leq 72^\circ$ ) while the vertical axis represents the diffraction intensity normalized to the maximum value. This graph reveals clearly the respective contributing intensities of the  $c_{\perp 10}$  and  $c_{\perp 160}$  components. After integration of each pole intensity and average of the three poles for each component, we found  $83 \pm 2\%$  of  $c_{\perp 10}$ , relative to the total volume of the presented sample. We estimated the deviation by integration over the zero-intensity ranges of the corrected pole figure on the same angle range as the poles. The angular dispersions are limited to  $4.5^\circ$  in  $\chi$  and  $4^\circ$  in  $\varphi$  at 15% of the maximum intensity. Thus, the sample exhibits a rather small mosaicity compared to usually grown ferroelectric materials such as perovskites<sup>[11]</sup> and the method of elaboration provides a texture of good quality even if in-plane misorientations are present.

Different assumptions can be expressed to understand these results. On one hand, the nucleation of the two variants described above can be explained as follows. The crystal structure for both lithium tantalate and sapphire can be visualized, along the  $c$ -axis direction, as a succession of oxygen octahedra with two thirds octahedral sites occupied by cations and the remaining one third left vacant. Figure 7

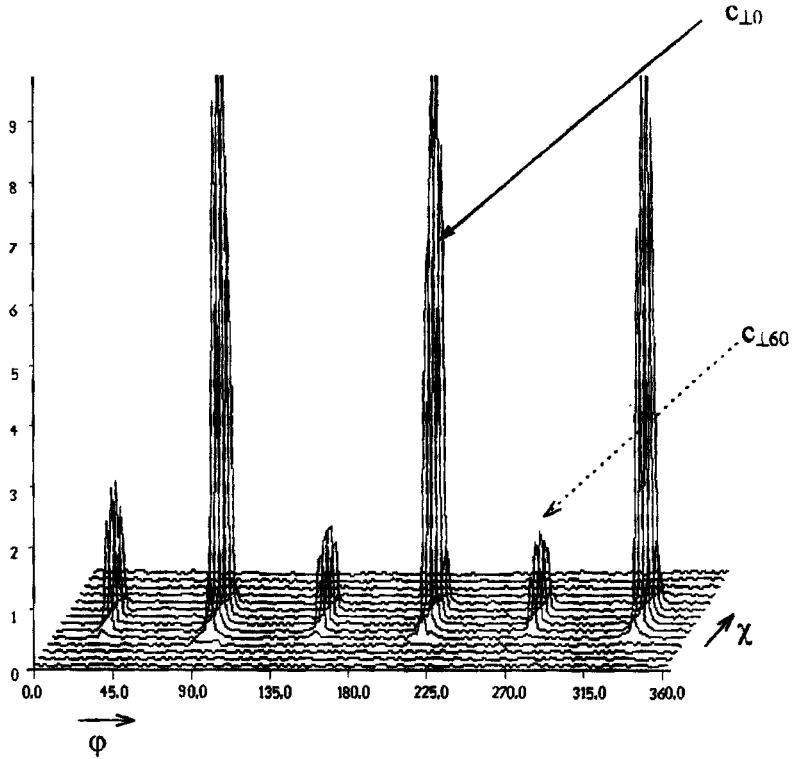


FIGURE 6 Three dimensional  $\varphi$  scan representation of the (012) pole figure of the Figure 4 [ $0 \leq \varphi \leq 360$ ],  $44^\circ \leq \chi \leq 72^\circ$ ,  $\Delta\varphi = 2^\circ$ ,  $\Delta\chi = 2^\circ$ .

shows a top view of the  $\{00l\}$  planes of  $\text{LiTaO}_3$  and  $\text{Al}_2\text{O}_3$ . The nucleation of lithium tantalate on this surface can occur by either the lithium or the tantalum atoms placed in the vacant octahedral sites. Since both lithium tantalate and sapphire are rhombohedral (three-fold symmetry), the two placements of lithium and tantalum can create orientations rotated by  $60^\circ$  with respect to one another. Thus, the growth from the two different nuclei results in two crystallographic variants in the film. On the other hand, the minor texture component could be provided by crystallites oriented with their  $c$ -axes in the opposite direction as those from the major component. In other words, the two crystallographic variants could be compared to parallel and anti-parallel domains. Then, a ratio of nearly 50% of  $c_{\perp 0}$  would



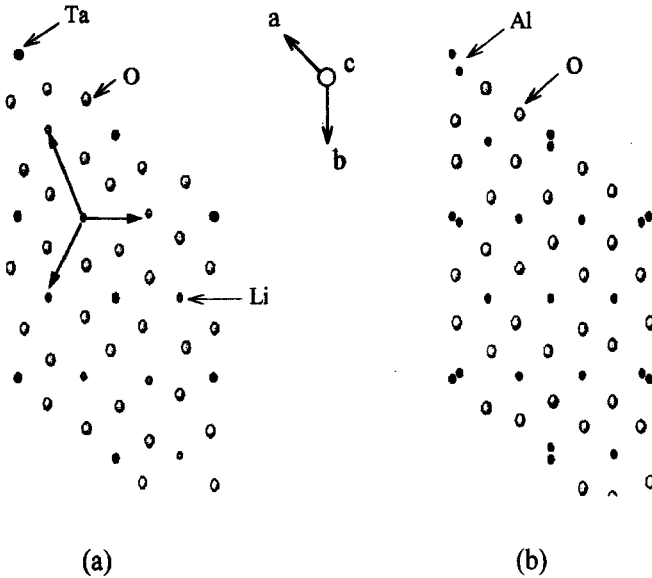


FIGURE 7 Top view of (a)  $\{00l\}$   $\text{LiTaO}_3$  (b)  $\{00l\}$   $\text{Al}_2\text{O}_3$ .

cancel any chance to observe piezoelectric properties, the  $c$ -axis direction being the polar-axis direction in this material. Thus, as the contribution of the two sets of poles is rather different, our strongly oriented  $\text{LiTaO}_3$  thin films could be sufficiently piezoelectric to form SAW filters, although strictly single crystalline films would be suitable.

## CONCLUSION

In summary, we have succeeded in growing strongly  $c$ -oriented thin films of single phase  $\text{LiTaO}_3$  by pyrosol process. The as-grown  $\text{LiTaO}_3$  layers exhibit a strong in-plane orientation with two components of different volumic ratio, thus showing good potentiality as new materials alternative in SAW devices.

## Acknowledgements

The authors acknowledge DRET/DGA and CNRS for their financial support.

**References**

- [1] Kanduser, A., Zigon, B., Mandrino, D., Kosec, M., Panjan, P. and Lavrenic, B. B. (1994). *Integrated Ferroelectrics*, **4**, 13.
- [2] Shibata, Y., Kuze, N., Matsui, M., Kanno, Y., Kaya, K., Ozaki, M., Kanai, M. and Kawai, T. (1995). *Jpn. P. Appl. Phys.*, **34**, 249.
- [3] Ye, C., Baude, P. and Polla, D. L. (1994). *Mater. Res. Soc. Symp. Proc.*, **321**, 603.
- [4] Retuert, P. J., Kneuer, P. G., Wittke, O., Avila, R. E. and Piderit, G. J. (1995). *J. Mater. Res.*, **10**(11), 2797.
- [5] Bornand, V., Papet, Ph. and Philippot, E. (1997). *Thin Solid Films*, **304**, 239.
- [6] Chateigner, D., Germi, P. and Pernet, M. (1994). *Mater. Sci. For.*, **157–163**, 1379.
- [7] Chateigner, D. (1994). *Thesis of the J. F. University, Grenoble*, p. 135.
- [8] Lotgering, F. K. (1959). *J. Inorg. Nucl. Chem.*, **9**, 113.
- [9] Agostinelli, J. A., Braunstein, G. H. and Blanton, T. N. (1993). *Appl. Phys. Lett.*, **63**(2), 123.
- [10] Schulz, L. G. (1949). *J. Appl. Phys.*, **20**, 1030.
- [11] Pernet, M., Chateigner, D., Germi, P., Dubourdieu, C., Thomas, O., Senateur, J. P., Chambonnet, D. and Belouet, C. (1994). *Physica C*, **235–240**, 627.